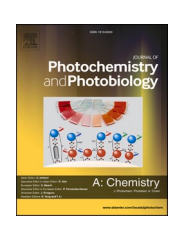
FISEVIER

Contents lists available at ScienceDirect

## Journal of Photochemistry & Photobiology, A: Chemistry

journal homepage: www.elsevier.com/locate/jphotochem





# Chlorin spiro-Tröger's base as a prospective photosensitizer for photodynamic therapy of cancer

Tereza Navrátilová<sup>a</sup>, Denisa Pineckerová<sup>b</sup>, Ameneh Tatar<sup>a</sup>, Ivana Křížová<sup>c</sup>, Martin Havlík<sup>a</sup>, Michaela Drozdová<sup>a</sup>, Jan Hajduch<sup>a</sup>, Jaroslav Zelenka<sup>b</sup>, Pavel Anzenbacher, Jr. <sup>d</sup>, Bohumil Dolenský<sup>a</sup>, <sup>\*</sup>

- <sup>a</sup> Department of Analytical Chemistry, University of Chemistry and Technology, Prague, 166 28 Prague 6, Czech Republic
- b Department of Biochemistry and Microbiology, University of Chemistry and Technology, Prague, 166 28 Prague 6, Czech Republic
- <sup>c</sup> Department of Biotechnology, University of Chemistry and Technology, Prague, 166 28 Prague 6, Czech Republic
- d Department of Chemistry, Bowling Green State University, Bowling Green, OH 43403, USA

#### ARTICLE INFO

#### Keywords: Tröger's base Spiro-Tröger's base Temoporfin Photodynamic therapy Porphyrinoid-sensitizer

#### ABSTRACT

Octahydroxy bis-porphyrin Tröger's base (TB) and octahydroxy porphyrin-chlorin spiro-Tröger's base (spiroTB) derivatives were successfully prepared from their Ni(II) complexes utilizing an optimized demetalation method using  $H_2SO_4$ -TFA followed by demethylation via BBr $_3$ . The synthesized TB and spiroTB were then in *in vitro* experiments for their utility in photodynamic therapy (PDT) of cancer. Compared to temoporfin (*m*THPC, Foscan®), the chlorin derivative used in PDT of cancer, TB and spiroTB were localized in lysosomes instead of the endoplasmic reticulum and were found to possess enhanced biocompatibility. Cell culture studies were performed on TRAMP-C2 (prostate cancer), HeLa (cervical cancer), and MRC-5 (non cancerous) cell lines. Both TB and spiroTB displayed negligible dark toxicity but increased production of reactive oxygen species (ROS) when illuminated. In addition, spiroTB displayed significant phototoxicity in TRAMP-C2 cells (IC<sub>50, light</sub> 0.7  $\mu$ M after 24 h incubation). Despite the phototoxicity of spiroTB being lower than that of *m*THPC (IC<sub>50, light</sub> 0.02  $\mu$ M), due to the low dark toxicity (IC<sub>50, dark</sub> > 100  $\mu$ M), the therapeutic factor of spiroTB (>150) is six times higher than that of *m*THPC (25).

### 1. Introduction

Photodynamic therapy (PDT) is an established treatment for various cancers, such as skin, lung, brain, bladder, pancreas, bile duct, esophagus, head and neck cancers, as well as other conditions, including acne and psoriasis and bacterial, fungal, and viral infections [1–4]. In general, PDT is based on the accumulation of a light-sensitive drug, the so-called photosensitizer, followed by irradiation with a light of suitable wavelength. The absorption of light then leads to the local production of reactive oxygen species (ROS), i.e., singlet oxygen or hydroxyl radicals, which subsequently cause the destruction of tumor cells, usually via apoptosis [5].

The ideal photosensitizer displays a high solubility in biological media, no dark toxicity, a high yield of ROS, selective accumulation in the targeted cells, and absorption of radiation in the so-called phototherapeutic window (650–850 nm) [6], where tissues have the lowest

absorption. Unfortunately, none of the known photosensitizers meets all the mentioned requirements [7]. Even the widely used 5,10,15,20-tetrakis(*m*-hydroxyphenyl)chlorin (temoporfin, *m*THPC, Foscan®, Scheme 1) [8] is far from being an ideal photosensitizer, e.g., *m*THPC must be stored at 20 °C due to the general instability of the unsubstituted chlorin core, is poorly soluble in biological media and exhibits rather high dark toxicity [1,9].

In 2012, we published our discovery that the conversion of  $\beta$ -amino [Ni]porphyrin to bis-porphyrin Tröger's base (TB) derivative  $1a\text{-Ni}_2$  is followed by the formation of chlorin-porphyrin spiro-Tröger's base (spiroTB) derivative  $2a\text{-Ni}_2$  [10], in which the chlorin moiety is stabilized by substitution on the reduced pyrrole (Scheme 1). The molecular structure of  $2a\text{-Ni}_2$  was proposed based on its similarity with the naphthalene spiroTB derivatives formed as by-products in TB preparation [11] (the only known spiroTB derivative before was derived from aminoazulene [12]). Recently, we reported confirmation of the structure

E-mail address: dolenskb@vscht.cz (B. Dolenský).

<sup>\*</sup> Corresponding author.

by electron diffraction and preparation of new derivatives, including spiroTB **2b-Ni<sub>2</sub>**, comprising *m*-methoxyphenyl moieties [13].

Thus, this study aimed to synthesize the yet unknown free base spiroTB **2c-H4**, which comprises the structural features of *m*THPC, investigate the photodynamic effect of this compound, and compare the photosensitization properties with the corresponding TB **1c-H4** congener and the parent *m*THPC. This comparison would shed light on the role of the TB and spiroTB moieties with respect to toxicity, photodynamic effects, and biological compatibility.

## 2. Results and discussion

## 2.1. Preparation of compounds

Preparations of the free base porphyrin TB derivatives  $1\text{-H}_4$  via direct troegeration of the free base  $\beta$ -aminoporphyrins with yields up to 70 % were first described by Crossley in 1995 [14]. However, spiroTB  $2\text{-H}_4$  derivatives were not reported, presumably because  $2\text{-H}_4$  were not formed or perhaps due to problems with their unambiguous identification.

Recently, published experiments aimed at directly preparing the free base of spiroTB 2b- $H_4$  were unsuccessful [13]. However, during the troegeration of tetrakis(3-methoxyphenyl)- $\beta$ -aminozinc(II)porphyrin under acidic conditions, simultaneous demetalation was observed, and free base 1b- $H_4$  was obtained in 35 % yield. Unfortunately, only traces of 2b- $H_4$  were formed. The difficulty with the isolation of 2b- $H_4$  presumably results from compound instability (vide infra).

Therefore, we prepared the free bases of both porphyrin TB  $1c\text{-H}_4$  and spiroTB  $2c\text{-H}_4$  by demethylation and demetalation of the TB  $1b\text{-Ni}_2$  and spiroTB  $2b\text{-Ni}_2$  derivatives (Scheme 2). We also tried the reverse procedure in which demethylation of the starting material was followed by demetalation, as well as first exchanging Ni(II) for Mg(II) followed by hydrolysis of the unstable Mg(II) complex. The latter attempts were unsuccessful. For more information, see ESI.

The first step of the preparation was demetalation of  ${\bf 2b}$ -Ni $_2$  in a mixture of H $_2$ SO $_4$  and TFA (1:20, v/v). The reaction was followed by TLC frequently and quenched immediately after the starting compound was consumed (approx. 30 min). After extraction with dichloromethane, the free base spiroTB  ${\bf 2b}$ -H $_4$  was obtained in 97 % yield. Because of the problems with purification,  ${\bf 2b}$ -H $_4$  was used in the next step without further purification. In the cases when the reaction was not quenched, complete decomposition of the products occurred within 45 min. The same treatment of a nickel(II) complex TB  ${\bf 1b}$ -Ni $_2$  yielded TB  ${\bf 1b}$ -H $_4$  in 84 % yield. Likewise, when the reaction is not quenched, a rapid decomposition occurs within 45 min.

The demethylation of  $2b\text{-H}_4$  in the second step was performed using boron tribromide in dichloromethane. The target spiroTB  $2c\text{-H}_4$  was obtained in 98 % yield in high purity (based on UV–Vis, fluorescence, and HRMS). Likewise, free base TB  $1b\text{-H}_4$  yielded TB  $1c\text{-H}_4$  in 98 % yield and purity > 95 % by LC–MS. Further, the *meso*-phenyl congeners TB  $1a\text{-H}_4$  (99 % yield) and spiroTB  $2a\text{-H}_4$  (98 % yield) with less hindered

Scheme 2. Preparation of targeted compounds 1c-H4 and 2c-H4.

rotation, which are easier to characterize by NMR, were prepared in 99 % and 98 % yield, respectively.

## 2.2. Stability and purification of the compounds

Various metal complexes, TBs  $1\text{-}M_2$  and spiroTBs  $2\text{-}M_2$ , were reported to be stable upon heating of their solutions up to  $145\,^{\circ}\text{C}$  [10,13] and purified by column chromatography on silica. However, their free base derivatives  $1\text{-}H_4$  and  $2\text{-}H_4$  prepared in this work showed significantly lower stability.

Although it was reported that 1a-H<sub>4</sub>, as well as its 3,5-di-tert-butylphenyl derivative were purified via chromatography [14], we found that chromatography of 1b-H<sub>4</sub> and 1c-H<sub>4</sub> on a normal phase silica column led to partial decomposition of the compounds (based on TLC, HRMS and  $^1H$  NMR). However, the prepared 1c-H<sub>4</sub> is obtained in > 95 % purity using reverse-phase HPLC. TBs 1-H<sub>4</sub> are thermally stable in solution in DMSO-d<sub>6</sub> even at 145 °C as determined by NMR spectra (Fig. S61, S68).

Unfortunately, the free base of porphyrin-chlorin spiroTB derivatives  ${\bf 2\text{-}H_4}$  were found to be less stable than their TB isomers  ${\bf 1\text{-}H_4}$ . The chromatography of  ${\bf 2a\text{-}H_4}$ ,  ${\bf 2b\text{-}H_4}$  and  ${\bf 2c\text{-}H_4}$  on silica led to a significant decomposition (TLC, HRMS and  ${}^1\text{H}$  NMR; e.g., Fig. S64). Decomposition was observed even on a reverse-phase column. HPLC-HRMS analysis of  ${\bf 2c\text{-}H_4}$  with a direct injection HRMS showed the formation of several new unknown products not observed in the original sample.

Moreover, the decomposition of  $2c\text{-H}_4$  at temperatures exceeding 40 °C in the presence of air was also observed. As expected for a photosensitizer, decomposition in the presence of light and air also took place. Fortunately, when stored under an argon atmosphere in a refrigerator without the presence of light,  $2c\text{-H}_4$  was found to be stable for up to six months in the form of a powder, a solution in DMF (based on identical UV–Vis spectra) and a solution in DMSO (based on repeatable biological tests).

It is worth noting that the first known spiroTB derived from 2-amino-azulene was described as unstable during column chromatography on alumina and melted with decomposition at 218–223  $^{\circ}$ C [12]. Similarly, naphth-2-ylamine spiroTB also melted with decomposition at 84–86  $^{\circ}$ C [17]. In contrast to the reported instability, spiroTBs derived from naphth-2-ylamines and anthracen-2-ylamine were stable [11]. Overall, these observations suggest that decomposition upon column chromatography and heating might be the common property of spiroTB derivatives.

## 2.3. Characterization of the compounds

The ordinary identification and characterization of the prepared

 $\mathbf{M} = \text{Ni, Zn or 2H; } \mathbf{a}) \text{ Ar = Ph, } \mathbf{b}) \text{ Ar = 3-MeO-Ph, } \mathbf{c}) \text{ Ar = 3-OH-Ph}$ 

Scheme 1. Molecular structures of the studied compounds.

spiroTBs **2b-H**<sub>4</sub> and **2c-H**<sub>4</sub> by NMR were severely complicated due to the limited rotation of the *meso*-aryl substituents, which can lead to the existence of up to 256 atropisomers. Therefore, recording well-resolved NMR spectra required measurements at temperatures exceeding the stability of the compounds (vide supra). Consequently, we also studied the derivatives **1a-H**<sub>4</sub> and **2a-H**<sub>4</sub> with unsubstituted phenyl groups as the *meso*-aryl substituents, which prevents the formation of atropisomers and results in less hindrance to phenyl rotation, thus lowering the coalescence temperatures of NMR signals.

All TB derivatives, 1a-H<sub>4</sub>, 1b-H<sub>4</sub>, and 1c-H<sub>4</sub>, were easily characterized by <sup>1</sup>H NMR spectra at higher temperatures. The <sup>1</sup>H signals of the methylene groups of 1a-H<sub>4</sub> were well resolved at 105 °C (Fig. S61), those of 1b-H<sub>4</sub> were well resolved at 145 °C [13], and those of 1c-H<sub>4</sub> were resolved at 120 °C. However, at least some signals of their *meso*-substituents were broadened even at temperatures approaching 150 °C (Fig. S61, S68, [13]). All the TB derivatives 1-H<sub>4</sub> were stable upon heating, as the <sup>1</sup>H NMR spectra before and after heating matched tightly. Further characterization of 1a-H<sub>4</sub>, 1b-H<sub>4</sub>, and 1c-H<sub>4</sub> was performed by recording the UV–Vis and fluorescence emission spectra at various concentrations. Their absorption maxima, absorption coefficients, and normalized fluorescence emission maxima were rather similar (Fig. 1, Table 1). Linear Lambert-Beer plots suggest that no intermolecular association is taking place.

Identification and characterization of the spiroTB derivatives 2a-H<sub>4</sub>, 2b-H<sub>4</sub>, and 2c-H<sub>4</sub> was more complicated. Their HRMS spectra contained intensive molecular ions corresponding to expected m/z, but the <sup>1</sup>H NMR spectra were rather complex. The <sup>1</sup>H NMR spectrum of 2a-H<sub>4</sub> confirmed the molecular structure at room temperature. The structure was better resolved above 100 °C. Still, some of the signals of the aromatic hydrogen atoms were very broad, even at 148 °C (Fig. S60-S61). Unfortunately, the <sup>1</sup>H NMR spectra of 2b-H<sub>4</sub> (Fig. S62) and 2c-H<sub>4</sub> (Fig. S66) were poorly resolved even at temperatures exceeding 100 °C, a consequence of atropisomerism and the slow rotation of the substituted phenyl groups. In addition, the NMR analyses were complicated by the decomposition of the compounds upon heating, as we observed by HRMS and NMR (Fig. S63, S67).

UV-Vis absorption and fluorescence emission spectra enabled comparison with **2a-H**<sub>4</sub> and were used to further confirm the molecular structures of **2b-H**<sub>4</sub> and **2c-H**<sub>4</sub> (Fig. 1, Table 1).

The UV–Vis spectra showed four Q-bands characteristic of free base porphyrinoids [18]. As is typical for the spiroTB derivatives 2-M<sub>2</sub> [10,13], the Soret band of **2c-H**<sub>4</sub> is located at 433 nm with a shoulder at 426 nm. The fluorescence emission spectrum of **2c-H**<sub>4</sub> displays a pattern

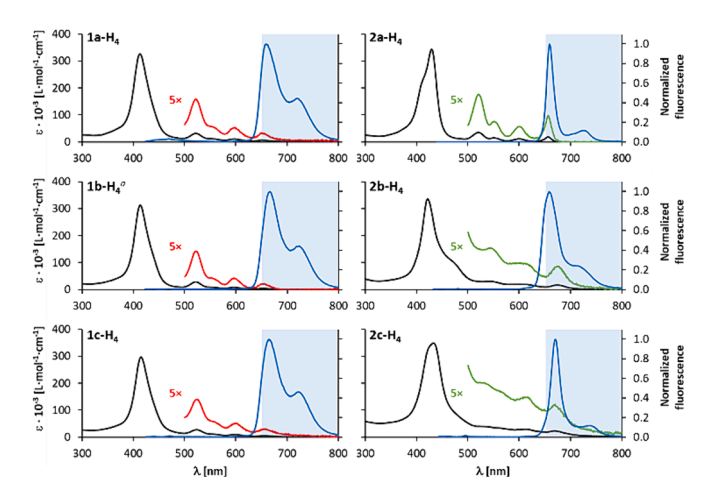


**Fig. 1.** UV–Vis absorption spectra of TBs **1-H**<sub>4</sub> (black–red) and spiroTBs **2-H**<sub>4</sub> (black–green) and normalized fluorescence emission spectra (blue) measured in DMF. The region of the phototherapeutic window (650–800 nm) is shown in blue. <sup>a</sup> Data from reference [13]. (For interpretation of the references to color in this figure legend, the reader is referred to the web version of this article.)

similar to that of spiroTB  $2a-H_4$ , including the ratio of both emission bands. Overall, the similarity of the UV–Vis and fluorescence emission spectra of  $2b-H_4$  and  $2c-H_4$  with that of  $2a-H_4$  (Fig. 1, Table 1) strongly supports the analogous molecular structure and purity. Moreover, the fluorescence intensity is low for all the compounds.

As expected, the UV–Vis spectra showed that all the prepared free base TBs and spiroTBs had absorption bands in the area of the phototherapeutic window. The targeted spiroTB  $2c-H_4$  had the fourth Q-band at 670 nm, which is 18 nm further in the phototherapeutic window than the commercial chlorin derivative mTHPC (Q4: 652 nm, in DMSO, Table 1) [19,20].

We attempted back metalation to further confirm the molecular structures of the free bases  $1b\text{-}H_4$  and  $2b\text{-}H_4$ . The back metalation of TB  $1b\text{-}H_4$  with nickel(II) acetate yielded the expected  $1b\text{-}Ni_2$ , which was identified by HRMS and by comparison with its TLC standard. Analogously, the zinc complex  $1b\text{-}Zn_2$  was obtained when zinc(II) acetylacetonate was used.

In contrast, the back metalation of spiroTB  $2b\text{-}H_4$  with nickel(II) acetate did not produce nickel(II) complex  $2b\text{-}Ni_2$  (based on TLC), but  $2b\text{-}Ni_1H_2$  was identified in the crude product by HRMS. Based on HRMS, back metalation using zinc(II) acetylacetonate yielded a complex mixture of products, including  $2b\text{-}Zn_2$ . SpiroTB derivatives are less stable than their TB isomers.

## 2.4. Toxicity and phototoxicity

Both 1c-H<sub>4</sub> and 2c-H<sub>4</sub> were found to be soluble in methanol, ethanol, DMF, DMSO and insoluble in water. The samples for biological evaluation were prepared by dissolving 1c-H<sub>4</sub> or 2c-H<sub>4</sub> in DMSO.

Mouse prostatic carcinoma TRAMP-C2 cells were treated with up to 100 μM 1c-H<sub>4</sub>, 2c-H<sub>4</sub>, or mTHPC in full media for 2 h and then irradiated with full-spectrum halogen light (emission maximum in the red region, water-filtered to avoid the heating effect, 15 min, 18 mW·cm<sup>-2</sup>) or kept in the dark, and their viability was analysed. The incubation time was set according to our experience with molecular photosensitizers [21,22]. However, none of the compounds exhibited phototoxicity or toxicity. Next, the incubation time was prolonged to 24 h in the dark, which is sufficient for slowly accumulating compounds [23]. In this setup, strong phototoxicity in the micromolar range was observed for 2c-H<sub>4</sub> but not for 1c-H<sub>4</sub>, and no dark toxicity was observed for either compound. However, strong submicromolar phototoxicity and considerable dark toxicity were observed for mTHPC. After dividing IC50 values for unwanted dark toxicity and desirable phototoxicity, a considerably broader therapeutic factor (>150) was observed for 2c-H<sub>4</sub> compared to that for mTHPC (25). Therefore, mTHPC is more effective, but spiroTB 2c-H<sub>4</sub> seems to be safer for patients.

In addition, the dark toxicity and phototoxicity were also determined in MRC-5 fibroblasts, a model of noncancerous cells, to evaluate the general value of  $\mathbf{2c}\text{-H}_4$  as a novel photosensitizer. The results showed that toxicity profiles were comparable between TRAMP-C2 and MRC-5, suggesting no clear selectivity to a particular genetic background. The longer exposure necessary for the application of  $\mathbf{2c}\text{-H}_4$  raised the question of whether it is caused by less efficient cells uptake or whether the transport is retarded by  $\mathbf{2c}\text{-H}_4$  binding to the serum proteins. Therefore, a two-hour incubation in the absence of fetal bovine serum prior to irradiation was examined. In this case, the IC50 values were comparable or slightly lower than those for 24-hour incubation in the presence of serum. Thus, significant binding to serum proteins was confirmed for all the investigated compounds. The IC50 values are summarized in Table 2. The original measurements of viability under different conditions are given in ESI (Fig. S80-S88).

## 2.5. Uptake and intracellular localization

The kinetics of porphyrin uptake by TRAMP-C2 cells were investigated using flow cytometry. Time- and dose-dependent uptake was

Table 1 UV–Vis absorption ( $\lambda_{max}$  in nm (log  $\epsilon$ )) and fluorescence emission characteristics of 1-H<sub>4</sub>, 2-H<sub>4</sub> and *m*THPC.

UV–Vis							Fluorescence		
	Soret bands	Q-bands					$\lambda_{em,1}$	$\lambda_{\text{em},2}$	
		IV	III	II	I				
1a-H <sub>4</sub>	413 (5.53)	523 (4.50)	555 (4.02)	598 (3.98)	652 (3.74)	413	658	720	
2a-H <sub>4</sub>	sh 411 (5.54) 429 (5.35)	520 (4.55)	551 (4.28)	601 (4.19)	657 (4.06)	429	660	728	
1b-H <sub>4</sub>	413 (5.49) <sup>a</sup>	$523 (4.45)^a$	$555 (3.93)^a$	$599 (3.91)^a$	$655 (3.59)^a$	413	667	725	
2b-H <sub>4</sub>	422 (5.50) sh 472 (4.97)	544 (4.45)	_b	603 (4.25)	674 (4.20)	422	660	717	
1c-H <sub>4</sub>	415 (5.47)	525 (4.45)	558 (4.06)	600 (4.02)	661 (3.76)	415	667	724	
2c-H <sub>4</sub>	sh 426 (5.48) 433 (5.49)	533 (4.54)	561 (4.47)	614 (4.40)	670 (4.31)	433	671	740	
mTHPC	421 (5.36) <sup>c</sup>	520 (4.27) <sup>c</sup>	546 (4.09) <sup>c</sup>	598 (3.85) <sup>c</sup>	652 (4.63) <sup>c</sup>	427 <sup>c</sup> 405 <sup>d</sup>	653 <sup>c</sup> 652 <sup>d</sup>	718 <sup>d</sup>	

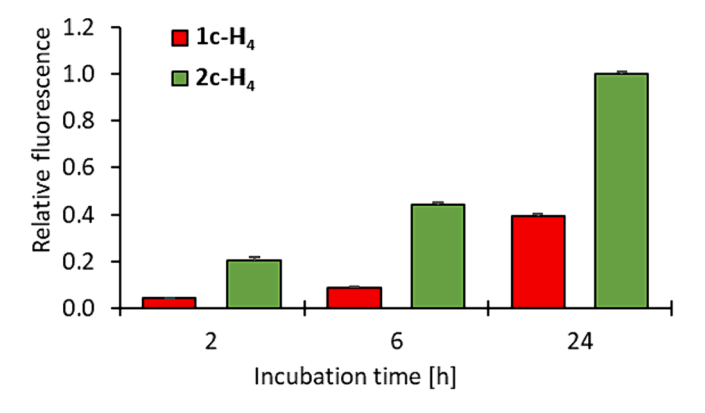
<sup>&</sup>lt;sup>a</sup>Data from reference [13]; <sup>b</sup>Overlap, <sup>c</sup>Data from reference [19], measured in DMSO, <sup>d</sup>Data from reference [20].

Table 2  $IC_{50}$  values calculated from the data measured on the TRAMP-C2 cell culture using the  $IC_{50}$  calculator [24].

	mTHPC		TB 1c-H <sub>4</sub>		spiroTB 2c-H <sub>4</sub>	
Incubation time [h]	24	2	24	2	24	2
Incubation [w/wo] <sup>a</sup> serum IC <sub>50,dark</sub> [µM] IC <sub>50,light</sub> [µM] Therapeutic factor	w 0.5 0.02 25	wo 3.9 0.03 130	w >100 62 >1.6	wo >100 >100 N. A. <sup>b</sup>	w >100 0.7 >150	wo >100 0.3 >330

 $<sup>^{</sup>a}$ w = with, wo = without;  $^{b}$ N. A. = not applicable.

observed for  $1c ext{-}H_4$  and  $2c ext{-}H_4$ , but  $2c ext{-}H_4$  signal was significantly stronger, suggesting a robust uptake. Therefore, the higher phototoxic efficiency of  $2c ext{-}H_4$  compared to that of  $1c ext{-}H_4$  may be explained by its more efficient uptake. Uptake of  $2c ext{-}H_4$  increases almost linearly with increasing concentration in the medium after 24 h of incubation, while  $1c ext{-}H_4$  seemed to saturate cells at lower concentrations (Fig. 2, top). The



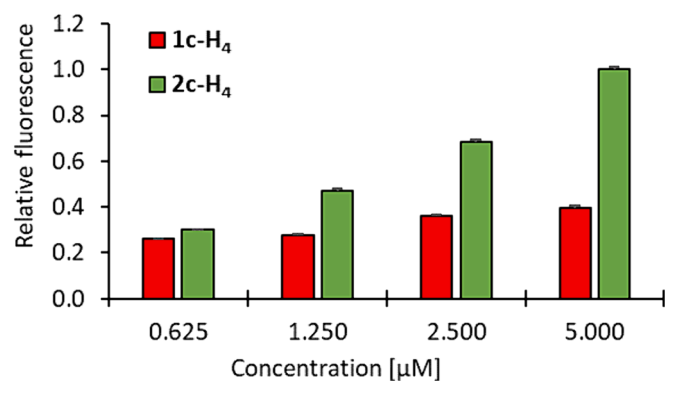


**Fig. 2.** Fluorescence measurements of **1c**-H<sub>4</sub> and **2c**-H<sub>4</sub> samples by flow cytometry. Top: Measured at different times of incubation (2, 6 or 24 h). Bottom: Measured at different concentrations of samples (0.625–5.000 µM).

uptake of both compounds increased linearly over time without reaching a plateau at 24 h (Fig. 2, bottom), suggesting that even several days of incubation may be necessary to reach equilibrium between intracellular and extracellular compartments. We may hypothesize that the preferential uptake of  $2c\text{-H}_4$  is caused by higher diffusion through plasmatic membrane or lower efflux by cellular detoxification pumps, which could be the consequence of specific structural features of spiroTB derivatives.

Confocal microscopy revealed that both 1c-H<sub>4</sub> and 2c-H<sub>4</sub> were selectively localized to lysosomes, which is a common property of porphyrins [25,26]. At the same time, *m*THPC was retained in the endoplasmic reticulum (Fig. 3). This difference could explain the lower dark toxicity of 2c-H<sub>4</sub> compared to that of *m*THPC since lysosomes are "trash bins" intended to store and decompose unwanted materials, while the endoplasmic reticulum is vital for cellular proteosynthesis. Moreover, damage to lysosomes after photoactivation can release digestive enzymes into the cytoplasm and trigger apoptosis [27].

Indeed, investigation of the cell death mode using flow cytometry and annexin/propidium iodide staining showed a dramatic increase in the apoptotic cell population after treatment with  $2c-H_4$  and irradiation compared to treatment with  $1c-H_4$  at the same concentration used for

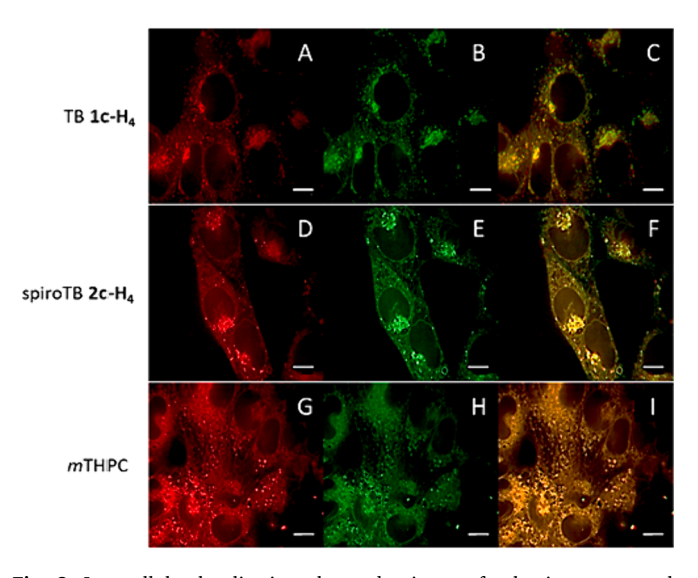


**Fig. 3.** Intracellular localization observed using confocal microscopy; scale bars: 10 μm. **A:** Localization of  $1c ext{-}H_4$  in the cell (red color); **B:** Lysosomes (LysoTracker green; green color); **C:** Overlay of images **A** and **B** (yellow color). **D:** Localization of  $2c ext{-}H_4$  in the cell (red color); **E:** Lysosomes (LysoTracker green; green color); **F:** Overlay of images **D** and **E** (yellow color). **G:** Localization of mTHPC in the cell (red color); **H:** Endoplasmic reticulum (ER tracker blue—white; green color); **I:** Overlay of images **G** and **H** (yellow color). (For interpretation of the references to color in this figure legend, the reader is referred to the web version of this article.)

**2c-H<sub>4</sub>**, while the necrotic population was negligible for all treatments (Fig. 4).

## 2.6. ROS production

The principal mechanism of photodynamic cell killing is producing reactive oxygen species (ROS) causing oxidative stress. However, cancer cells can counteract oxidative stress due to the upregulation of antioxidant mechanisms [28]. Oxidative stress results in elevation of intracellular ROS caused by antioxidant depletion, radical chain reaction, and damage of metabolic enzymes. We intended to measure intracellular ROS levels as a marker of cellular oxidative damage. Thus, ROS levels in the cells treated with porphyrins after irradiation were visualized using specific ROS-sensitive probes. All three compounds increased the ROS levels compared to the controls, and the ROS signal was stronger for **2c**-H<sub>4</sub> than for **1c**-H<sub>4</sub> (Fig. 5).

## 3. Conclusion

Three free base porphyrin-chlorin spiroTB derivatives were prepared, expanding the small family of spiroTB compounds. SpiroTB  $2c-H_4$  was prepared, its photochemical properties were investigated, and the compound was evaluated with respect to a potential use as a photosensitizer in photodynamic therapy (PDT). This compound compares favourably with the commercial chlorin derivative mTHPC currently used in PDT of certain cancers under the brand name Foscan®.

Studies of the photophysical and photochemical properties of octahydroxy bis-porphyrin Tröger's base (TB **1c-H**<sub>4</sub>) and octahydroxy porphyrin-chlorin spiro-Tröger's base (spiroTB **2c-H**<sub>4</sub>) and comparison with a similar tetrahydroxy-derivative, *m*THPC, revealed redshifted absorption spectra and higher absorption coefficients for these porphyrin derivatives compared to those for *m*THPC. While the bisporphyrin TB **1c-H**<sub>4</sub> shows only a negligible photodynamic effect, owing to the chlorin moiety, the new porphyrin-chlorin compound spiroTB **2c-H**<sub>4</sub> displays a high phototoxicity in the submicromolar range and a very low dark toxicity. As a result, the therapeutic factor of spiroTB **2c-H**<sub>4</sub> is six times higher than that of *m*THPC, which displays high dark toxicity.

Subcellular localization studies show that spiroTB  $2c\text{-H}_4$  and TB  $1c\text{-H}_4$  are localized in lysosomes, while mTHPC is preferentially localized in the endoplasmic reticulum. The different subcellular localization is presumably due to the diazocine moiety. These structural features will be explored further and aimed at developing new chlorin spiroTB derivatives that will display low dark toxicity and higher stability so that they could be a safer alternative in porphyrin (chlorin)-based photodynamic therapy of cancer.

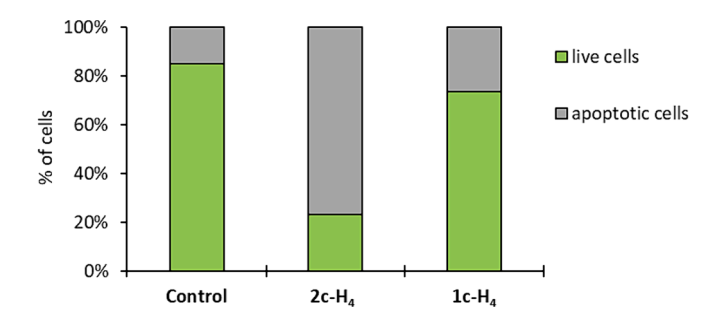


Fig. 4. Investigation of the cell death mode using flow cytometry: ratios of live and apoptotic cells.

#### 4. Experimental section

#### 4.1. Materials

All reagents were purchased from commercial suppliers and used without further purification. The tested batch of *m*THPC (Temoporfin, Item: 17333, Batch: 0494841-20, 25 mg, crystalline solid, >95 % pure by HPLC analysis) was purchased from Cayman Chemical Company (USA). Starting compounds **1a-Ni<sub>2</sub>**, **2a-Ni<sub>2</sub>**, **1b-Ni<sub>2</sub>**, and **2b-Ni<sub>2</sub>** were prepared according to our previously published procedures [13]. Chromatography-grade silica (32-63 D, 60 Å) was used to purify the prepared compounds. The final compound **1c-H<sub>4</sub>** was >95 % pure by HPLC. The high purity of **2c-H<sub>4</sub>** was confirmed by UV–Vis and fluorescence emission spectra since the compound decomposed during chromatography (vide supra). For detailed preparation of all compounds, including comments on stability, see ESI.

# 4.2. General procedure for the synthesis of compounds $1a-H_4$ , $2a-H_4$ , $1b-H_4$ and $2b-H_4$

The appropriate nickel(II) complex ( $1a\text{-Ni}_2$ ,  $2a\text{-Ni}_2$ ,  $1b\text{-Ni}_2$  or  $2b\text{-Ni}_2$ ) was dissolved in a 20:1 (v/v) mixture of TFA and conc.  $H_2SO_4$  in a round bottom flask. The solution was stirred at RT. After 30 min, the reaction mixture was poured onto ice water; the solution was rendered basic with 25 % aq·NH $_3$  and extracted with  $CH_2Cl_2$ . The combined organic layers were washed with water, dried over anhydrous  $Na_2SO_4$  and evaporated to dryness. The targeted compounds ( $1a\text{-H}_4$ ,  $2a\text{-H}_4$ ,  $1b\text{-H}_4$ , and  $2b\text{-H}_4$ ) were obtained as crystalline compounds without further purification.

## 4.2.1. Phenyl TB derivative (1a-H<sub>4</sub>)

Red-brown crystalline compound; yield 99 % (11 mg).  $^1$ H NMR (500 MHz, DMSO- $^4$ 6, 145 °C):  $\delta$  8.70 (d, 2H, J = 5.0 Hz), 8.67 (d, 2H, J = 5.0 Hz), 8.56 (d, 2H, J = 5.0 Hz), 8.50 (d, 2H, J = 5.0 Hz), 8.34 (d, 2H, J = 5.0 Hz), 8.15-7.98 (m, 11H), 7.89–7.67 (m, 20H), 7.65–7.50 (m, 9H), 4.64 (s, 2H), 4.19 (d, 2H, J = 17.5 Hz), 4.11 (d, 2H, J = 17.5 Hz), ~3.0 (s br, cov., 2H), -2.82 (s br, 2H). HRMS (ESI $^+$ ): calcd. for [C<sub>91</sub>H<sub>62</sub>N<sub>10</sub> + H] $^+$  1295.52317, found 1295.52405, calcd. for [C<sub>91</sub>H<sub>62</sub>N<sub>10</sub> + Na] $^+$  1317.50511, found 1317.50574, calcd. for [C<sub>91</sub>H<sub>62</sub>N<sub>10</sub> + K] $^+$  1333.47905, found 1333.47961.  $\lambda$ <sub>max</sub>/nm (log  $\epsilon$ <sub>max</sub>) in DMF: 413 (5.53), 523 (4.50), 555 (4.02), 598 (3.98), 652 (3.74).

## 4.2.2. Phenyl spiroTB derivative (2a-H<sub>4</sub>)

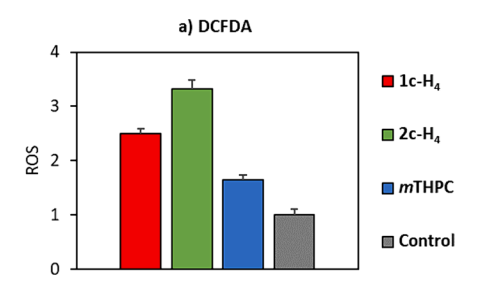
Dark green brown crystalline compound; yield 98 % (9.0 mg).  $^{1}$ H NMR (500 MHz, DMSO- $^{1}$ 6, 148 °C):  $\delta$  8.77 (d, 1H, J = 4.8 Hz), 8.76 (d, 1H, J = 4.8 Hz), 8.72 (d, 1H, J = 4.8 Hz), 8.66 (d, 1H, J = 4.8 Hz), 8.63 (d, 1H, J = 4.8 Hz), 8.61 (d, 1H, J = 4.8 Hz), 8.59 (d, 1H, J = 4.8 Hz), 8.43 (d, 1H, J = 4.8 Hz), 8.41 (m, 2H), 8.31–8.02 (m, 13H), 7.90 (d, 2H, J = 7.7 Hz), 7.84 (m, 21H), 7.48 (d, 2H, J = 7.7 Hz), 6.81 (t, 1H, J = 7.5 Hz), 6.68 (t, 1H, J = 7.5 Hz), 4.54 (d, 1H, J = 18.3 Hz), 4.26 (d, 1H, J = 18.3 Hz), 3.82 (d, 1H, J = 17.9 Hz), 3.74 (d, 1H, J = 12.0 Hz), 3.30 (d, 1H, J = 17.9 Hz), 3.20 (d, 1H, J = 12.0 Hz), 1.48 (s br, 2H), -2.55 (s br, 2H). HRMS (ESI $^+$ ): calcd. for  $[C_{91}H_{62}N_{10} + H]^+$  1295.52317, found 1395.52295, calcd. for  $[C_{91}H_{62}N_{10} + K]^+$  1317.50511, found 1317.50452, calcd. for  $[C_{91}H_{62}N_{10} + K]^+$  1333.47905, found 48.26434.  $\lambda_{max}$ /nm (log  $\varepsilon_{max}$ ) in DMF: 429 (5.54), 411 (5.35), 520 (4.55), 551 (4.28), 601 (4.19), 657 (4.06).

## 4.2.3. m-Methoxyphenyl TB derivative (1b-H<sub>4</sub>)

Red-brown crystalline compound; yield 84 % (7.8 mg). The spectroscopic data were in agreement with our previous work [13].

## 4.2.4. m-Methoxyphenyl spiroTB derivative (2b- $H_4$ )

Dark green brown crystalline compound; yield 97 % (9.0 mg). HRMS (ESI $^+$ ): calcd. for [ $C_{99}H_{78}N_{10}O_8+H$ ] $^+$  1535.60769, found 1535.60840,



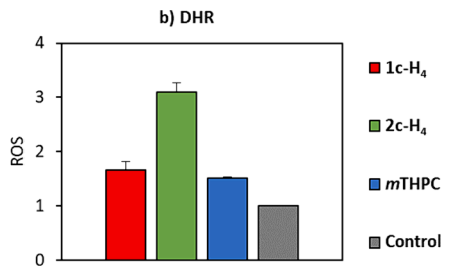


**Fig. 5.** ROS levels in TRAMP-C2 cells after treatment with photosensitizers followed by irradiation. Concentrations of the samples: TB **1c-H<sub>4</sub>** and spiroTB **2c-H<sub>4</sub>**: 2.5 μM, *m*THPC: 0.08 μM. Incubation: 24 h, with serum. a) 2′,7′-Dichlorodihydrofluorescein diacetate (DCFDA) was used as a ROS sensitive probe; b) dihydrorhodamine (DHR) was used as a ROS sensitive probe.

calcd. for  $[C_{99}H_{78}N_{10}O_8+N_a]^+$  1557.58963, found 1557.58984, calcd. for  $[C_{99}H_{78}N_{10}O_8+K]^+$  1573.56357, found 1573.56946, calcd. for  $[C_{99}H_{78}N_{10}O_8+2H]^{2+}$  768.30748, found 768.30676.  $\lambda_{max}/nm$  (log  $\epsilon_{max}$ ) in DMF: 422 (5.50), 472 (4.97), 544 (4.45), 603 (4.25), 674 (4.20). For  $^1H$  NMR spectra see Fig. S65-66.

## 4.3. General procedure for the synthesis of compounds $1c-H_4$ and $2c-H_4$

The appropriate free base (1b-H<sub>4</sub> or 2b-H<sub>4</sub>, 1 eq.) was dissolved in dry CH<sub>2</sub>Cl<sub>2</sub> (20 mL) in a round bottom flask wrapped with aluminum foil, and an argon atmosphere was established. The solution was cooled to 0 °C, and boron tribromide (5.5 eq. of BBr<sub>3</sub> per 1 MeO group) was added dropwise. The reaction mixture was left to reach room temperature and allowed to proceed overnight. The next day, the reaction was cooled to 0 °C and quenched by slowly adding ice-cooled water. The resulting suspension was dissolved in a small amount of methanol. The solution was extracted using CH2Cl2/H2O. The precipitate on the intermediate phase was filtered on a frit. The precipitate was washed with hexane and dissolved in a small amount of methanol. Then, 25 % aq·NH<sub>3</sub> was added to the solution, and the resulting solution was evaporated to dryness. The crude product was dissolved in diethyl ether and extracted with water. The organic layer was separated and dried over anhydrous Na<sub>2</sub>SO<sub>4</sub> in an Erlenmeyer flask covered with aluminum foil. The targeted compound (1c-H<sub>4</sub> or 2c-H<sub>4</sub>) was obtained as a solid after evaporation of the organic layer without further purification. The work-up was performed as fast as possible to avoid excessive contact with light and air.

## 4.3.1. m-Hydroxyphenyl TB derivative (1c-H<sub>4</sub>)

Red brown solid; yield 98 % (134 mg).  $^1\text{H}$  NMR (500 MHz, DMSO- $d_6$ , 145 °C):  $\delta$  9.18 (s br, 3H), 9.00 (s br, 2H), 8.88–8.69 (m, 6H), 8.64 (d, 2H, J=4.8 Hz), 8.57 (d, 2H, J=4.8 Hz), 8.42 (d, 2H, J=4.8 Hz), 8.24 (d, 2H, J=4.8 Hz), 7.81–6.96 (m, 32H), 4.74 (s, 2H), 4.40 (d, 2H, J=17.8 Hz), 4.32 (d, 2H, J=17.8 Hz), -2.93 (s br, 4H). HRMS (ESI+): calcd. for  $[\text{C}_{91}\text{H}_{62}\text{N}_{10}\text{O}_8 + \text{H}]^+$  1423.48249, found 1423.48352, calcd. for  $[\text{C}_{91}\text{H}_{62}\text{N}_{10}\text{O}_8 + \text{Na}]^+$  1445.46443, found 1445.46472, calcd. for  $[\text{C}_{91}\text{H}_{62}\text{N}_{10}\text{O}_8 + \text{K}]^+$  1461.43837, found 1461.43787, calcd. for  $[\text{C}_{91}\text{H}_{62}\text{N}_{10}\text{O}_8 + \text{ZH}]^{2+}$  712.24488, found 712.24420.  $\lambda_{\text{max}}/\text{nm}$  (log  $\epsilon_{\text{max}}$ ) in DMF: 415 (5.47), 525 (4.45), 558 (4.06), 600 (4.02), 661 (3.76).

## 4.3.2. m-Hydroxyphenyl spiroTB derivative (2c- $H_4$ )

Purple brown solid; yield 98 % (52 mg). HRMS (ESI<sup>+</sup>): calcd. for  $[C_{91}H_{62}N_{10}O_8 + H]^+$  1423.48249, found 1423.48096, calcd. for  $[C_{91}H_{62}N_{10}O_8 + Na]^+$  1445.46443, found 1445.46289, calcd. for  $[C_{91}H_{62}N_{10}O_8 + 2H]^{2+}$  712.24488, found 712.24402.  $\lambda_{max}$ /nm (log  $\epsilon_{max}$ ) in DMF: 426 sh (5.48), 433 (5.49), 533 (4.54), 561 (4.47), 614 (4.40), 670 (4.31). For  $^1H$  NMR spectra see Figs. S69-70.

## 4.4. NMR spectroscopy

The NMR spectra were recorded using a 500.16 MHz instrument (JEOL, Tokyo, Japan). The chemical shifts ( $\delta$ ) are given in ppm. The  $^1$ H

chemical shifts are referenced using the residual solvent signals ( $^{1}$ H NMR: DMSO- $d_{6}$  2.50 ppm, TCE- $d_{2}$  5.91 ppm) at all temperatures.

## 4.5. UV-Vis spectroscopy

The electronic absorption spectra were recorded in a 1 cm optical quartz cuvette (Aireka Cells) on a Cary 60 UV–Vis spectrometer (Agilent Technologies) in the 190–1100 nm wavelength range. Samples for the measurement were dissolved in DMF. The UV–Vis spectra were obtained by dividing the measured spectra from the dilution experiments by the measured concentration and then averaging the spectra thus obtained. The spectra were processed by blank subtraction (DMF). The molar absorption coefficients of the prepared compounds were determined by linear regression from dilution experiments.

#### 4.6. Fluorescence spectroscopy

The fluorescence emission spectra were measured in a 1 cm quartz cuvette (Aireka Cells) on a Cary Eclipse fluorescence spectrometer (Agilent Technologies) using DMF as a solvent. The spectra were obtained by averaging the normalized fluorescence emission spectra measured at two different concentrations. The Soret band wavelength was used as the excitation wavelength for each compound.

## 4.7. Mass spectrometry

Mass spectrometry was performed using an LTQ Orbitrap Velos mass spectrometer (Thermo Scientific), a hybrid Ion trap - Orbitrap spectrometer with an Ion Max ion source and H-ESI II probe. The conditions for MS detection were as follows: ionization: ESI $^+$ , spray voltage: 3.0 kV, source temperature: 250 °C, capillary temperature: 300 °C, measurement mode: FTMS, resolution (FWHM): 30000, lock mass: 413.2662 Da (diisooctyl phthalate), and scan: 150–2000 Da. Samples were dosed under direct injection conditions (FIA) using an Accela 600 (Thermo Scientific) pump. The conditions for the injection were as follows: sample dosage: 5  $\mu$ l (injection loop, Rheodyne valve), mobile phase: methanol, and flow of mobile phase: 150  $\mu$ l/min.

## 4.8. High-performance liquid chromatography

The purities of compounds  $1c\text{-H}_4$  and  $2c\text{-H}_4$  were followed via reversed-phase HPLC using an analytical-size (250  $\times$  4.0 mm) Reprosil 100 C18 column (5  $\mu$ m, Watrex, Czech Republic) at 25 °C. The separations were monitored using a UV–Vis detector at a wavelength of 254 nm and recorded using Clarity software. The samples for analyses were dissolved in HPLC-grade methanol. Samples were introduced via an injection loop (20  $\mu$ l) with an 10  $\mu$ l injection volume. The concentration of the samples was 1.0 mg/mL. The separation conditions for  $1c\text{-H}_4$  were 1.0–5.0 min: gradient elution, 100 % MeOH; and mobile phase flow rate: 0.250 mL/min. The separation conditions for  $2c\text{-H}_4$  were 1.0–30.0

min: isocratic elution, 100 % MeOH; and mobile phase flow rate: 0.500 mL/min.

The purity of compound  $2c\text{-}H_4$  was further followed via reversed-phase HPLC/MS. For HPLC, an analytical-size (50  $\times$  2.1 mm) Hypersil GOLD^TM C18 column (1.9  $\mu\text{m}$ , Thermo Scientific, USA) was used. The separation conditions were as follows: sample dosage: 5  $\mu\text{l}$  (injection loop, Rheodyne valve), isocratic elution, and mobile phase: methanol, the of mobile phase: 300  $\mu\text{l}/\text{min}$ . The sample for analysis was dissolved in HPLC-grade methanol. The conditions for MS detection were as follows: ionization: ESI+, spray voltage: 3.0 kV, source temperature: 350 °C, measurement mode: FTMS, resolution (FWHM): 30000, lock mass: 413.2662 Da (diisooctyl phthalate), and scan: 200–2000 Da.

## 4.9. Cell cultures

TRAMP-C2 – mouse prostate adenocarcinoma cells were cultured in a complete medium consisting of DMEM (Dulbecco's modified Eagle medium), 5 % Nu-serum, 5 % serum, 1 % penicillin/streptomycin, insulin, and trans-dehydroandrosterone (DHEA) at 37 °C under a 5 %  $\rm CO_2$  atmosphere. MRC-5 – human fibroblasts isolated from lung tissue were cultured in a complete medium consisting of EMEM medium (Eagle's minimal essential medium), 5 % serum, and 0.5 mM glutamine at 37 °C under a 5 %  $\rm CO_2$  atmosphere. HeLa – human cervical adenocarcinoma cells were cultured in a complete medium consisting of EMEM medium, 5 % serum, and 0.5 mM glutamine at 37 °C under a 5 %  $\rm CO_2$  atmosphere.

## 4.10. Toxicity and phototoxicity

The experiments were performed on two different cell lines -TRAMP-C2 and MRC-5. Experiments were performed under three different conditions: 24-hour incubation in medium with serum, 2-hour incubation in medium with serum, and 2-hour incubation in the medium without serum. Compounds (1c-H<sub>4</sub>, 2c-H<sub>4</sub> and mTHPC) were dissolved in DMSO, and then equal volumes with different concentrations of compounds were added to the cells in medium. The final concentration of DMSO in the cells was not higher than 1 % v/v DMSO. Before the compounds were added, the medium was replaced with fresh full medium without phenol red. After the incubation of cells with 1c-H<sub>4</sub>, 2c- $H_4$ , and mTHPC for 24 h (or 2 h) in the dark, the cells were kept in the dark or irradiated (with a halogen lamp in the presence of water heat filtration, 18 mW·cm<sup>-2</sup>, full-spectrum halogen light) for 15 min. Next, the samples were again replaced with fresh full medium and incubated for 24 h. The evaluation was performed 24 h after changing the medium. Cell viability was analysed using resazurin (Sigma Aldrich) and the results were visually controlled by microscopy. Viability results were related to controls with identical concentration of serum and DMSO and identical incubation time.

## 4.11. Flow cytometry

TRAMP-C2 cells were seeded in 12-well culture plates. The day before the measurement, four different concentrations of  $1c\text{-H}_4,\,2c\text{-H}_4,$  and mTHPC were added to the cells to determine the concentration dependence. Equal concentrations of  $1c\text{-H}_4,\,2c\text{-H}_4,$  and mTHPC (5  $\mu\text{M})$  were added to other cells 2 h and 6 h before the start of the measurement to determine the time dependence. Both tests were performed on TRAMP-C2 cell cultures in a medium with serum. The incubation time was 24 h.

For the measurement of cell death, HeLa cells treated with 1c-H<sub>4</sub> and 2c-H<sub>4</sub>, irradiated, and incubated for 5 h were resuspended in annexin binding buffer and labeled with annexin V FITC Alexa Fluor 488 and propidium iodide (Invitrogen), and stained cells (ten thousand events) were analyzed using BD FACSDiva 8 software on a BD FACSAria III flow cytometer. The incubation time was 24 h. After irradiation (15 min, halogen lamp, full-spectrum halogen light), the medium was changed. The evaluation took place 6 h after irradiation. The concentration of

both  $1c\text{-}H_4$  and  $1c\text{-}H_4$  was 5  $\mu\text{M}.$  The excitation wavelength in flow cytometry was 405 nm.

## 4.12. Confocal microscopy

TRAMP-C2 cells (incubation time: 24 h) were seeded on a black 96-well culture plate, and subsequently,  $1c\text{-H}_4$ ,  $2c\text{-H}_4$ , and mTHPC were added to them (concentration of the samples: 5  $\mu\text{M}$ ). The localization of the compounds was visualized with an Andor xD spinning disk confocal microscope on an Olympus IX81 platform. The excitation and emission wavelengths were 405 nm and 700 nm for the porphyrin derivatives and 488 nm and 535 nm for the used probes.

#### 4.13. ROS measurement

TRAMP-C2 cells (incubation time: 24 h) were seeded on a black 96-well culture plate, and subsequently, **1c-H<sub>4</sub>**, **2c-H<sub>4</sub>**, and *m*THPC were added to them (concentration of the samples: **1c-H<sub>4</sub>**, and **2c-H<sub>4</sub>**: 2.5  $\mu$ M, *m*THPC: 0.08  $\mu$ M). After 24 h, the cells were irradiated with a halogen lamp in the presence of water heat filtration, 18 mW·cm<sup>-2</sup> for 15 min. ROS-sensitive probes 2′,7′-dichlorodihydrofluorescein diacetate (DCFDA) and dihydrorhodamine (DHR) were added, and their fluorescence ( $\lambda_{ex}$  488 nm/ $\lambda_{em}$  525 nm) was monitored after 1 h of incubation.

## CRediT authorship contribution statement

Tereza Navrátilová: Writing – original draft, Investigation, Data curation. Denisa Pineckerová: Writing – original draft, Investigation, Data curation. Ameneh Tatar: Writing – review & editing, Investigation. Ivana Křížová: Writing – review & editing, Investigation. Martin Havlík: Writing – review & editing, Supervision. Michaela Drozdová: Writing – review & editing. Jan Hajduch: Writing – review & editing. Jan Hajduch: Writing – review & editing, Supervision. Pavel Anzenbacher: Writing – review & editing, Supervision, Funding acquisition. Bohumil Dolenský: Writing – review & editing, Supervision, Funding acquisition, Conceptualization.

## Declaration of competing interest

The authors declare that they have no known competing financial interests or personal relationships that could have appeared to influence the work reported in this paper.

## Data availability

Data will be made available on request.

## Acknowledgements

This work was supported by the Ministry of Education, Youth and Sports of the Czech Republic (program INTER-EXCELLENCE, project no. LTAUSA19065) and by the National Science Foundation (NSF CHE 2102581 to PA).

## Appendix A. Supplementary data

Supplementary data to this article can be found online at https://doi.org/10.1016/j.jphotochem.2024.115618.

#### References

 I. Yakavets, M. Millard, V. Zorin, H.P. Lassalle, L. Bezdetnaya, Current state of the nanoscale delivery systems for temoporfin-based photodynamic therapy: Advanced delivery strategies, J. Controlled Release 304 (2019) 268–287, https://doi.org/ 10.1016/j.jconrel.2019.05.035.

- [2] A. Wiehe, J.M. O'Brien, M.O. Senge, Trends and targets in antiviral phototherapy, Photochem. Photobiol. Sci. 18 (2019) 2565–2612, https://doi.org/10.1039/c9 pp00211a
- [3] G. He, M. He, R. Wang, X. Li, H. Hu, D. Wang, Z. Wang, Y. Lu, N. Xu, J. Du, J. Fan, X. Peng, W. Sun, A near-infrared light-activated photocage based on a ruthenium complex for cancer phototherapy, Angew. Chem., Int. Ed. 62 (e202218768) (2023) 1–9. https://doi.org/10.1002/anje.202218768.
- [4] X.-Q. Zhou, P. Wang, V. Ramu, L. Zhang, S. Jiang, X. Li, S. Abyar, P. Papadopoulou, Y. Shao, L. Bretin, M.A. Siegler, F. Buda, A. Kros, J. Fan, X. Peng, W. Sun, S. Bonnet, In vivo metallophilic self-assembly of a light-activated anticancer drug, Nat. Chem. 15 (2023) 980–987, https://doi.org/10.1038/s41557-023-01199-w.
- [5] T. Mishchenko, I. Balalaeva, A. Gorokhova, M. Vedunova, D.V. Krysko, Which cell death modality wins the contest for photodynamic therapy of cancer? Cell Death Dis. 13 (455) (2022) 1–16, https://doi.org/10.1038/s41419-022-04851-4.
- [6] T.P. Kubrak, P. Kolodziej, J. Sawicki, A. Mazur, K. Koziorowska, D. Aebisher, Some natural photosensitizers and their medicinal properties for use in photodynamic therapy, Molecules 27 (1192) (2022) 1–19, https://doi.org/10.3390/ molecules27041192.
- [7] J.M. Dabrowski, B. Pucelik, A. Regiel-Futyra, M. Brindell, O. Mazuryk, A. Kyziol, G. Stochel, W. Macyk, L.G. Arnaut, Engineering of relevant photodynamic processes through structural modifications of metallotetrapyrrolic photosensitizers, Coord. Chem. Rev. 325 (2016) 067–101, https://doi.org/10.1016/j.ccr.2016.06.007
- [8] A. Wiehe, M.O. Senge, The photosensitizer temoporfin (mTHPC) chemical, preclinical and clinical developments in the last decade, Photochem Photobiol. 99 (2023) 356–419, https://doi.org/10.1111/php.13730.
- [9] M.O. Senge, J.C. Brandt, Temoporfin (Foscan®, 5,10,15,20-Tetra(m-hydroxy-phenyl)chlorin) A Second-generation Photosensitizer, Photochem. Photobiol. 87 (2011) 1240–1296, https://doi.org/10.1111/j.1751-1097.2011.00986.x.
- [10] A. Tatar, B. Dolenský, H. Dvořáková, V. Král, Selective formation of either Tröger's base or spiro Tröger's base derivatives from [2-amino-porphyrinato(2)]nickel by choice of reaction conditions, Tett. Lett. 53 (2012) 6015–6017, https://doi.org/ 10.1016/j.tetlet.2012.08.097.
- [11] A. Tatar, J. Čejka, V. Král, B. Dolenský, Spiro Tröger's Base Derivatives: Another Structural Phoenix? Org. Lett. 12 (2010) 1872–1875, https://doi.org/10.1021/ ol1004774
- [12] T. Okujima, T. Terazono, S. Ito, N. Morita, T. Asao, Reaction of 2-aminoazulenes with aldehydes. One pot synthesis of diazuleno[2,1-b:1,2-e]pyridines, Heterocycles 54 (2001) 667–678, https://doi.org/10.3987/COM-00-S(I)42.
- [13] T. Navrátilová, A. Tatar, M. Havlík, J. Hajduch, M. Drozdová, K. Gurung, L. Palatinus, J. Čejka, J. Sedláček, P. Anzenbacher Jr., B. Dolenský, Preparation and characterization of metalloporphyrin Tröger's and Spiro-Tröger's base derivatives, J. Org. Chem. 87 (2022) 15178–15186, https://doi.org/10.1021/acs.joc.2c01716.
- [14] M.J. Crossley, T.W. Hambley, L.G. Mackay, A.C. Try, R. Walton, Porphyrin analogues of Troger's base; large chiral cavities with a bimetallic binding site.

- J. Chem. Soc., Chem. Commun. (1995) 1077–1079, https://doi.org/10.1039/C39950001077.
- [17] M. Havlík, T. Navrátilová, M. Drozdová, A. Tatar, P.A. Lanza, D. Dusso, E. L. Moyano, C.A. Chesta, D.M.A. Vera, B. Dolenský, Experimental, spectroscopic, and computational insights into the reactivity of "Methanal" with 2-naphthylamines, Molecules 28 (1549) (2023) 1–19, https://doi.org/10.3390/pubm.land.20041540
- [18] Giovannetti, R. The Use of Spectrophotometry UV-Vis for the Study of Porphyrins. In Macro to Nano Spectroscopy, Uddin, J., Ed.; IntechOpen: London, 2012.
- [19] Y.-H. Gao, V. Lovreković, A. Kussayeva, D.-Y. Chen, D. Margetić, Z.-L. Chen, The photodynamic activities of dimethyl 131-[2-(guanidinyl)ethylamino] chlorin e6 photosensitizers in A549 tumor, Eur. J. Med. Chem. 177 (2019) 144–152, https://doi.org/10.1016/j.ejmech.2019.05.050.
- [20] W. Alian, S. Andersson-Engels, K. Svanberg, S. Svanberg, Laser-induced fluorescence studies of meso-tetra(hydroxyphenyl)chlorin in malignant and normal tissues in rats, Br. J. Cancer 70 (1994) 880–885, https://doi.org/10.1038/ bic.1994.414.
- [21] K. Kirakci, J. Zelenka, I. Křížová, T. Ruml, K. Lang, Octahedral molybdenum cluster complexes with optimized properties for photodynamic applications, Inorg. Chem. 59 (2020) 9287–9293, https://doi.org/10.1021/acs.inorgchem.0c01173.
- [22] K. Kirakci, J. Zelenka, M. Rumlová, J. Cvačka, T. Ruml, K. Lang, Cationic octahedral molybdenum cluster complexes functionalized with mitochondriatargeting ligands: photodynamic anticancer and antibacterial activities, Biomater. Sci. 7 (2019) 1386–1392, https://doi.org/10.1039/ C8RM01564C
- [23] J. Hynek, M. Koncošová, J. Zelenka, I. Křížová, T. Ruml, P. Kubát, J. Demela, K. Lang, Phosphinatophenylporphyrins tailored for high photodynamic efficacy, Org. Biomol. Chem. 16 (2018) 7274–7281, https://doi.org/10.1039/ C80R01984C
- [24] AAT Bioquest, Inc. (2022, December 5). Quest Graph™ IC<sub>50</sub> Calculator. AAT Bioquest. https://www.aatbio.com/tools/ic50-calculator.
- [25] T.M. Tsubone, W.K. Martins, C. Pavani, H.C. Junqueira, R. Itri, M.S. Baptista, Enhanced efficiency of cell death by lysosome-specific photodamage, Sci. Rep. 7 (6734) (2017) 1–19, https://doi.org/10.1038/s41598-017-06788-7.
- [26] K.W. Woodburn, N.J. Vardaxis, J.S. Hill, A.H. Kaye, D.R. Phillips, Subcellular localization of porphyrins using confocal laser scanning microscopy, Photochem. Photobiol. 54 (1991) 725–732, https://doi.org/10.1111/j.1751-1097.1991. tb02081.x.
- [27] D. Kessel, J.J. Reiners, Photodynamic therapy: autophagy and mitophagy, apoptosis and paraptosis, Autophagy 16 (2020) 2098–2101, https://doi.org/ 10.1080/15548627.2020.1783823.
- [28] J. Zelenka, M. Koncošová, T. Ruml, Targeting of stress response pathways in the prevention and treatment of cancer, Biotechnol. Adv. 36 (2018) 583–602, https:// doi.org/10.1016/j.biotechadv.2018.01.007.